Journal of Alloys and Compounds 509 (2011) 2132–2136

Contents lists available at ScienceDirect

Journal of Alloys and Compounds

journal homepage: www.elsevier.com/locate/jallcom

Synthesis of Sm–Co and Sm–Co/Fe nanocrystals by reductive annealing of nanoparticles

Girija S. Chaubey, Narayan Poudyal, Yuzi Liu, Chuanbing Rong, J. Ping Liu*

Department of Physics, University of Texas at Arlington, Arlington, TX 76019, United States

ARTICLE INFO

Article history:
Received 14 July 2010
Received in revised form 22 October 2010
Accepted 27 October 2010
Available online 4 November 2010

Keywords:
Nanoparticle
Annealing
Nanocomposite
Magnetic properties

ABSTRACT

We report here a simple route for the chemical synthesis of $SmCo_5$ and Sm_2Co_{17} single-phase and $SmCo_5$/Fe composite nanocrystals by polyol reduction of metal precursors and subsequent calcium reductive annealing. Sm_2O_3 and Co nanoparticles were synthesized first, and nanocrystalline $SmCo_5$ or Sm_2Co_{17}, compound with tunable composition was then obtained after the annealing. The composition of the compound was controlled by varying the initial molar ratio of the metal precursors. At room temperature, the obtained $SmCo_5$ and Sm_2Co_{17} show coercivity of 12 kOe and 4 kOe, and saturation magnetization of 70 emu/g and 85 emu/g, respectively. To prepare $SmCo_5$/Fe nanocomposites, Fe, Co and Sm_2O_3 nanoparticles were synthesized in one-pot by polyol reduction of the metal precursors.

1. Introduction

Rare-earth-transitional-metal compounds exhibit magnificent magnetic and optical properties. In particular, Sm–Co compounds have superior intrinsic magnetic properties such as very high Curie temperatures and magnetocrystalline anisotropy, and therefore are applied as high performance permanent magnets and are expected to be applied in high-density magnetic recording media [1,2]. For permanent magnet applications, exchange-coupled nanocomposite magnets containing magnetically hard/soft phases with high energy product $(BH)_{max}$ are desirable [3–6]. The intimate contact between the hard phase with high coercivity and the soft phase with high magnetization results in a high energy product due to the inter-phase exchange-coupling. However, synthesis of Sm–Co based nanocomposite remains a challenging task due to the poor chemical stability of the Sm-containing nanoparticles. Several techniques such as ball milling [7–10], melt spinning [11–13], electrodeposition [14,15] and spark plasma sintering [16] were developed for fabrication of Sm–Co based nanostructured magnets. However, preparation of Sm–Co nanostructured magnets with controllable nanoscale grain size and narrow size distribution still remains a challenge. Numerous attempts to synthesize $SmCo_5$ nanoparticles with high-temperature reductive decomposition of organometallic precursors have been reported [17–19], though no room-temperature magnetic hysteresis was reported until a two-step synthetic strategy was developed by us to prepare $SmCo_5$ nanocrystals by reductive annealing of the Co@Sm_2O_3 core/shell nanoparticles [20]. It was reported that, by properly tuning the dimension of the Sm_2O_3 shell, different phases of Sm–Co system can be obtained after the annealing. By adding Fe_3O_4 nanoparticles into the Sm–Co–O matrix before the annealing, SmCo/Fe nanocomposite nanocrystals were produced [21]. Recently, Matsushita et al. have synthesized $SmCo_5$ nanoparticles using polyol method with room temperature coercivity of 1500 Oe [22]. One of the major hurdles for the synthesis of SmCo alloy is its high reactivity towards oxygen when exposed to air. The oxidation kinetics and oxidation morphology of SmCo alloy were recently reported [23,24]. A high density gas aggregation nanoparticle gun [25] and several other synthetic efforts to make SmCo alloy and SmCo-based nanocomposites [26] have also been reported recently.

In this paper, we report a simple method to synthesize $SmCo_5$ (or Sm_2Co_{17}) and $SmCo_5$/Fe composite nanocrystals with well controlled composition and grain size by high temperature reduction of metal and metal oxide nanoparticles.

2. Experimental procedures

All the reagents used in this synthesis are commercially available. Iron (III) acetylacetonate ($Fe(acac)_3$), cobalt (II) acetylacetonate ($Co(acac)_2$), 1,2-hexadecanediol (HDD), trioctylphosphine (TOP) and oleic acid were purchased from Sigma–Aldrich. Samarium (III) acetylacetonate ($Sm(acac)_3$) was obtained from Strem Chemical. Calcium powder was purchased from American Element Company. All the reactions were carried out under inert atmosphere.

2.1. Synthesis of Sm_2O_3 and Co nanoparticles

$Co(acac)_2$ (1 mmol, 0.257 g), $Sm(acac)_3$ (0.2 mmol, 0.09 g), 1,2-hexadecanediol (3 mmol, 0.77 g) and oleic acid (3 ml) were charged to 125 ml round bottom flask at

* Corresponding author. Tel.: +1 817 272 2815; fax: +1 817 272 3637.
E-mail address: pliu@uta.edu (J.P. Liu).

0925-8388/$ – see front matter © 2010 Published by Elsevier B.V.
doi:10.1016/j.jallcom.2010.10.164

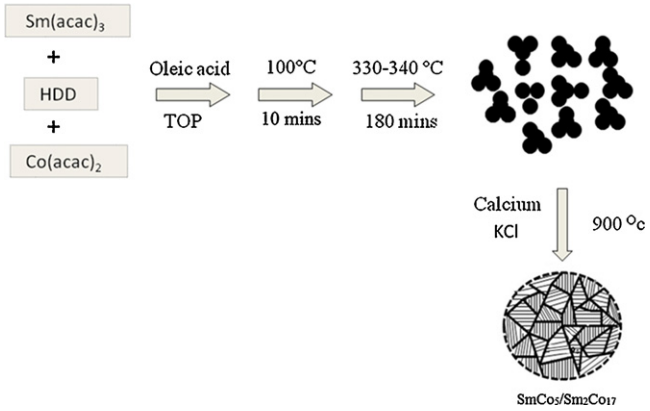

Scheme 1. Schematic illustration of synthesis of nanocrystalline $SmCo_5$ or Sm_2Co_{17} from the mixture of Co and Sm_2O_3 nanoparticles.

room temperature. After purging with argon for 30 min, trioctylphosphine (2.7 ml) was injected and the reaction mixture was heated to 100 °C for 10 min. Subsequently, the reaction mixture was heated to a temperature in the range 330–340 °C and refluxed for 3 h. Argon gas was flowed through out the reaction. Most of the surfactants were evaporated and a black dense product was obtained by adding 20 ml of ethanol and centrifugation. The product was washed 2–3 times using mixture of hexane (10 ml) and ethanol (40 ml) and separated via centrifugation. Finally, Sm_2O_3 and Co nanoparticles having an average diameter of 25 nm were redispersed in hexane.

2.2. Synthesis of Sm_2O_3, Co and Fe nanoparticles

$Co(acac)_2$ (2 mmol, 0.514 g), $Sm(acac)_3$ (0.4 mmol, 0.18 g), 1,2-hexadecanediol (8 mmol, 2.06 g) and oleic acid (5 ml) and an appropriate amount of $Fe(acac)_3$ were charged to a 125 ml round bottom flask at room temperature. After purging with argon for 30 min, trioctylphosphine (2.7 ml) was injected and the reaction mixture was heated to 100 °C for 30 min. The reaction was then heated to 330–340 °C and refluxed for 3 h before cooling down to room temperature. 20 ml of ethanol was added to the product and centrifuged to separate the black product. The product was then washed 2–3 times with hexane and ethanol and separated via centrifugation. Finally, a nanoparticle mixture comprising of Sm_2O_3, Co and Fe were obtained.

2.3. Synthesis of $SmCo_5$, Sm_2Co_{17} nanomagnets and $SmCo_5$/Fe nanocomposite magnets

Dried powder of the as-synthesized Sm_2O_3 and Co nanoparticles or Sm_2O_3, Co and Fe nanoparticles (300 mg) were ground together with potassium chloride (150 mg) and calcium powder (450 mg) and mixed thoroughly inside an inert-gas glove box. The mixture was then loaded in an iron boat and transferred to a tube furnace. The tube was purged with the forming gas (Ar + 7% H_2) for 30 min. The furnace was first heated to 120 °C for 30 min and then to 900 °C for 1–1.5 h under continuous flow of the forming gas. The ash colored product was then washed several times with deionized water to remove Ca, CaO and KCl powders. Finally, the products $SmCo_5$, or Sm_2Co_{17}, or $SmCo_5$/Fe were obtained. Schemes 1 and 2 show the synthesis routes for the formation of $SmCo_5$ or Sm_2Co_{17} nanocrystals and $SmCo_5$/Fe nanocomposites, respectively.

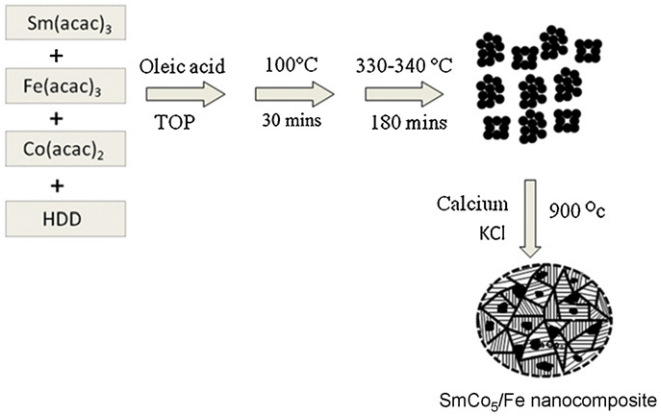

Scheme 2. Schematic illustration of synthesis of nanocrystalline $SmCo_5$/Fe nanocomposite from the mixture of Co, Fe and Sm_2O_3 nanoparticles. Black spot represent Fe nanograins in $SmCo_5$ matrix.

Our extended experiments showed that this method can be potentially scalable for large scale production. This synthetic strategies involved one-pot synthesis of mixture of nanoparticles. By simply multiplying the amount of the precursors in designated molar ratio, large scale nanoparticles can be obtained.

The morphology of the nanoparticles was observed using transmission electron microscopy (TEM). Samples for TEM analysis were prepared by drying a hexane dispersion of the particles on amorphous carbon coated copper grids. X-ray diffraction (XRD) patterns of the particle assemblies were collected on a diffractometer with Cu K-α radiation (λ = 1.5406 Å). Magnetic measurements were carried out using a superconducting quantum interference device (SQUID) magnetometer. The composition analysis was done by energy dispersive X-ray spectroscopy (EDX) and coupled plasma-atomic emission spectroscopy (ICP-AES).

3. Results and discussion

The reductive thermal decomposition of $Co(acac)_2$ and $Fe(acac)_3$ in the presence of surfactants resulted in formation of Co and Fe nanoparticles where as Sm_2O_3 nanoparticles was formed by the thermal decomposition of $Sm(acac)_3$. Oleic acid and trioctylphospine were capping ligands to stabilize the nanoparticles and 1,2-hexadecanediol was reducing agent. Fig. 1A shows the TEM image of as-synthesized mixture of Sm_2O_3 and Co nanoparticle assemblies and Fig. 1B shows a TEM image of Co, Fe and Sm_2O_3 nanoparticles in flower-like assemblies.

Fig. 2A shows XRD patterns of Sm_2O_3 and Co samples in different stages. The pattern (a) is for as-synthesized sample, one can only find peaks corresponding to Co phase, indicating that Sm_2O_3 may be in an amorphous state. To confirm the presence of Sm_2O_3, the as-synthesized sample was annealed at 900 °C in nitrogen atmosphere. XRD measurement of the annealed sample confirmed the presence of both Sm_2O_3 and Co in the sample (Fig. 2A(b)). To obtain hard magnetic Sm–Co phase, the nanoparticles were annealed at 900 °C in presence of calcium. It is obvious that the Sm_2O_3 particles were reduced and diffused into cobalt nanoparticles to form the hard magnetic Sm–Co phases. Similar result was obtained when Co/Sm_2O_3 core/shell nanoparticles were annealed at 900 °C with calcium [20].

The final composition of the Sm/Co was controlled by tuning the initial molar ratio of the Sm and Co metal precursors. For example, the atomic ratio of Co to Sm with values of 86 to 14 or 90 to 9 was obtained by feeding an initial molar ratio of 5:1 and 9:1 for Co and Sm metal precursors, respectively. Slight deviation in the final composition of Sm/Co ratio from their initial precursor's molar ratio is due the minimal evaporation of Sm during annealing process. The final composition of the particle was determined by EDX and ICP-AES.

However, the grain size of the resulted Sm–Co particles is quite large because of the high annealing temperature. In order to control the grain growth, we added potassium chloride (KCl) salt, similar as our previously reported salt-matrix annealing method [27,28], into the mixture of Sm_2O_3, Co nanoparticles and calcium powder and then heat treated the mixture at 900 °C in forming gas. It was observed that presence of KCl salt reduces grain growth effectively, due to the fact that the salt impedes interdiffusion between the particles. In the mean time, large amount of KCl salt also slowered down the reduction of the Sm_2O_3 nanoparticles. We varied weight ratio of Sm_2O_3, Co, Ca and KCl to optimize the composition and annealing conditions and found that the ratio in weight of 2:3:1 between Sm_2O_3 and Co nanoparticles, Ca and KCl resulted in a best control of grain growth while having a complete Sm oxide reduction. The ash colored product was then washed several times with deionized water to remove Ca, CaO and KCl powders. Fig. 2A(c, d) shows the XRD patterns of the samples after the reductive annealing. The diffraction peaks matched well with the standard $SmCo_5$ and Sm_2Co_{17} patterns (JCPDS No. 35-1400 and JCPDS No. 35-1368), indicating that high temperature reduction and interface diffusion lead to the formation of hexagonal structured $SmCo_5$ and Sm_2Co_{17} phases, respectively. The average grain size calculated from the

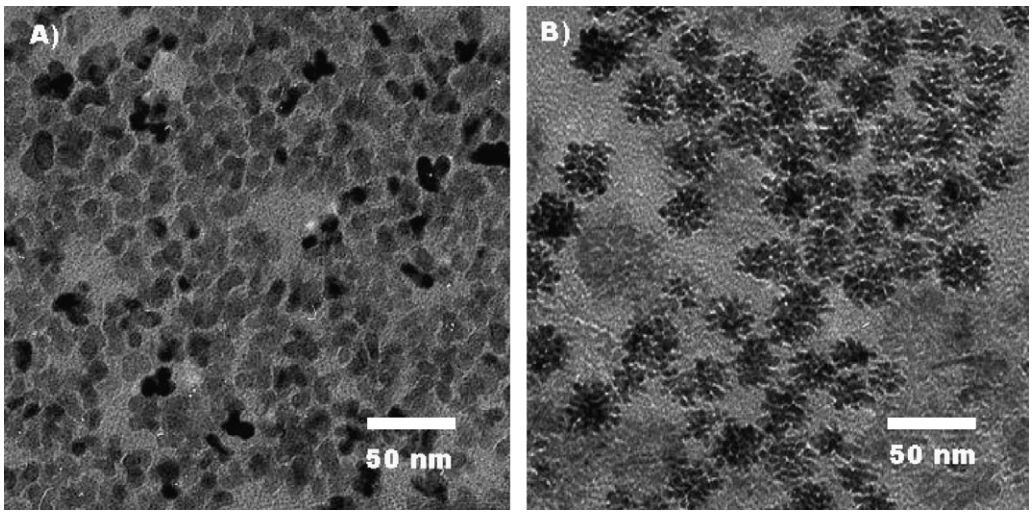

Fig. 1. Bright-field TEM images of (A) as-synthesized Co and Sm_2O_3 nanoparticles and (B) as-synthesized Co, Fe and Sm_2O_3 nanoparticles.

XRD patterns using the Scherrer equation [29] is 25 nm for $SmCo_5$ phase and 28 nm for Sm_2Co_{17} phase. Few very low intensity peaks are present in Fig. 2A(d), this could be due to the trace amount of Sm_2O_3 in the sample. Fig. 2B shows the typical HRTEM image of $SmCo_5$ nanocrystals obtained after the high-temperature reduction annealing. The interfringes spacing of 0.29 nm was observed in each nanocrystal grain which corresponds to the (1 0 1) planes of the $SmCo_5$ phase. SAED patterns further confirmed the $SmCo_5$ phase (not shown here).

Exchange-coupled magnets are nanocomposites that are composed of magnetically hard and soft phases that interact by magnetic exchange coupling. The synthesis of single phase Sm–Co nanocrystals was further extended to synthesize $SmCo_5$/Fe nanocomposites by modifying the synthesis procedure. The synthesis procedure of $SmCo_5$/Fe nanocomposite was similar to $SmCo_5$ particles synthesis except that Fe $(acac)_3$ was added to the reaction mixture as a Fe-source in addition to Sm and Co metal precursors, as shown in Scheme 2. Under present reaction condition, the formation of FeCo alloy [30] is unlikely due to the presence of Sm_2O_3 nanoparticles which hinders atomic diffusion of Fe and Co. It was reported earlier that the exchange-coupled $SmCo_5$/Fe nanocomposite can be obtained [21] by reductive annealing of the mixture of Sm–Co-O and Fe_3O_4 nanoparticle.

TEM image of the as-synthesized nanoparticles of Co, Fe and Sm_2O_3 is shown in Fig. 1B. It can be seen that nanoparticles of size in the range 5–10 nm were self-assembled together to form flower-like assemblies. X-ray diffraction measurement on the as-synthesized sample confirmed the presence of Fe and Co (Fig. 3A). Sm_2O_3 peaks were not observed in the as-synthesized sample due to its amorphous nature as discussed earlier.

The proportion of Fe nanoparticles in the final product can be controlled by varying the initial molar ratio of the iron-precursor while keeping the Sm and Co precursor molar ratio constant. Upon reductive annealing at 900 °C in presence of Ca and KCl salt-matrix, nanocomposite $SmCo_5$/Fe was obtained [21]. The sample was in powder form having micron size $SmCo_5$ particles containing nanocrystals of $SmCo_5$ and Fe. High resolution TEM analysis of the annealed powder sample shows the presence of both typical Sm–Co and Fe nanocrystals grains. It can be seen from Fig. 3B that the sample consists of nanoscale grains of two phases as indicated by dash lines, one with lattice fringe distance at 0.29 nm and another at 0.20 nm, corresponding to the (1 0 1) planes in the $SmCo_5$ and the (1 1 0) planes in bcc-Fe, respectively. This was further confirmed by the XRD analysis (Fig. 3A). XRD patterns revealed that the slight diffusion of Fe into $SmCo_5$ during the reductive annealing resulted in the formation of Sm_2Co_{17} phase [21]. Fe peak was

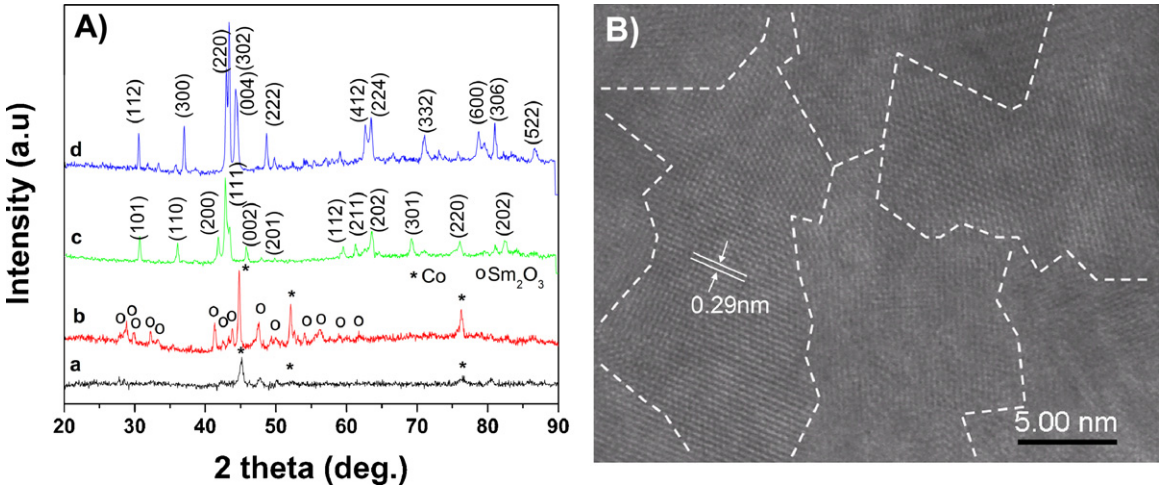

Fig. 2. (A) X-ray diffraction patterns of (a) as-synthesized mixture of Co and Sm_2O_3 nanoparticles (b) mixture Co and Sm_2O_3 nanoparticles annealed at 900 °C in nitrogen atmosphere and (c) nanocrystalline $SmCo_5$ (d) nanocrystalline Sm_2Co_{17}, prepared by reductive annealing of mixture of Co and Sm_2O_3 nanoparticles (B) HRTEM image of the nanocrystalline $SmCo_5$ product.

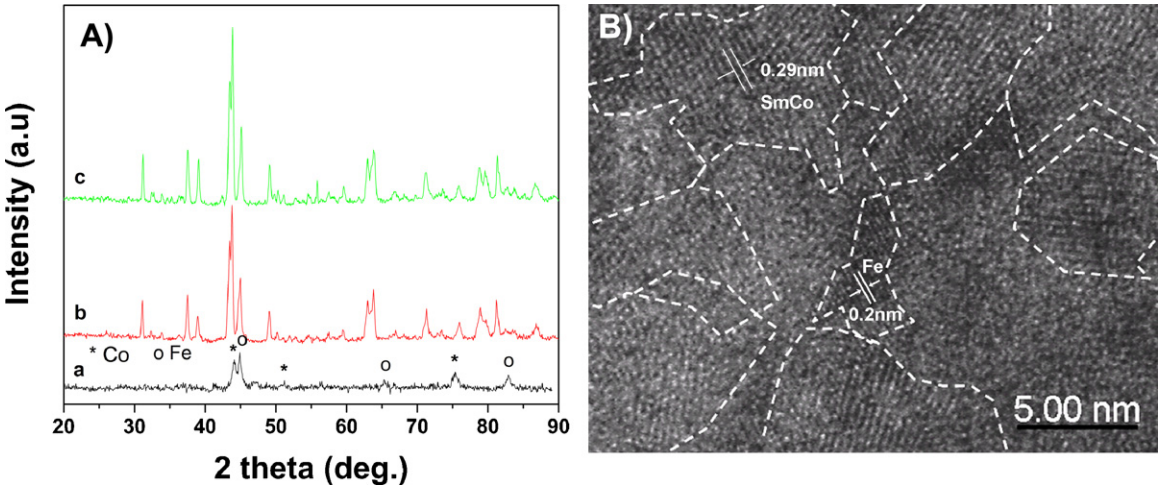

Fig. 3. (A) X-ray diffraction patterns of (a) as-synthesized Co, Fe and Sm_2O_3 nanoparticles mixture (b) $SmCo_5Fe_{0.6}$ (c) $SmCo_5Fe_{1.2}$ nanocomposite (B) HRTEM image of an assembly of nanocrystalline $SmCo_5$/Fe structure, with dashed lines showing the nanocrystalline grain boundaries of either Sm–Co or Fe.

difficult to characterize in these X-ray diffraction patterns as its (1 1 0) peak is overlapped with Sm_2Co_{17} (0 0 4) peak. However, it can be clearly seen in Fig. 3A that the intensity corresponding to (1 1 0) peak of bcc-Fe increases with increasing Fe fraction in the nanocomposite providing additional evidence of presence of Fe in the nanocomposite.

Fig. 4 shows room temperature hysteresis loops of the $SmCo_5$ nanocrystals and $SmCo_5$/Fe nanocomposite. It can be seen that the coercivity up to 12 kOe and saturation magnetization of 70 emu/g was obtained for $SmCo_5$. The room-temperature magnetic hysteresis loops for $SmCo_5$/Fe nanocomposite are also shown in Fig. 4. It can be seen that with increasing Fe fraction in the nanocomposite, the coercivity decreases whereas magnetization increases. The energy products $(BH)_{max}$ are about 6.0, 7.1 and 7.8 MGOe for $SmCo_5$, $SmCo_{5.5}Fe_{0.6}$ and $SmCo_{6.5}Fe_{1.2}$, respectively. A strong positive peak in the δM plot suggested the strong exchange coupling interaction between the nanograins of the hard and soft phases (as shown in Fig. 5) [31]. However, the intercept of *x*-axis in δM plot is higher than the coercivity of $SmCo_5$/Fe nanocomposite indicating not homogeneous distribution of soft fraction in nanocomposite sample. By optimizing the soft fraction in $SmCo_5$/Fe nanocomposite, the exchange coupling between two magnetic phases can be further increase and hence the squareness of the magnetic loops and the energy products can be improved. The consolidation experiments on these nanocomposite materials are under investigation.

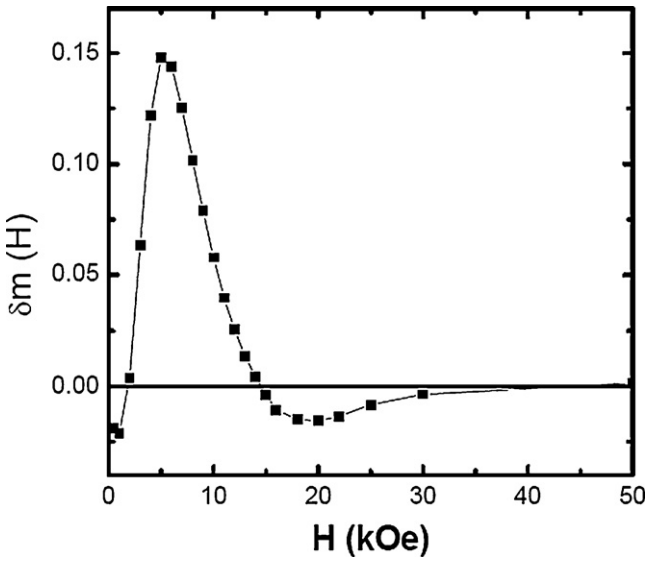

Fig. 5. The δM plot for $SmCo_5$/Fe nanocomposite.

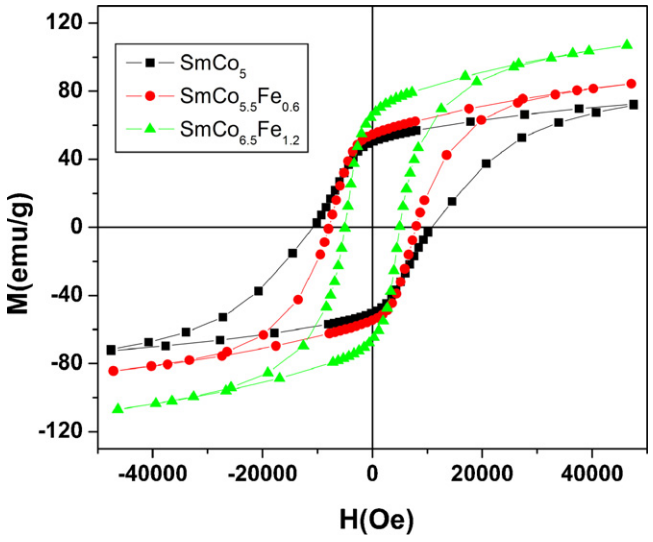

Fig. 4. Room temperature magnetic hysteresis loops of nanocrystalline $SmCo_5$ and $SmCo_5$/Fe nanocomposite.

4. Conclusions

In summary, a simple procedure for synthesis of $SmCo_5$ and Sm_2Co_{17} nanocrystals and $SmCo_5$/Fe nanocomposites has been reported. The room-temperature magnetic coercivity of 12 kOe was obtained for $SmCo_5$ nanostructure. Addition of Fe nanoparticles resulted in exchange-coupled $SmCo_5$/Fe nanocomposites. The increase of Fe fraction in $SmCo_5$/Fe composite has resulted in a decrease in coercivity and an increase in saturation magnetization. The reported synthetic procedures are easily scalable for large scale production.

Acknowledgements

This work was supported by US DoD/MURI grant N00014-05-1-0497. This work was also supported by the Center of

Nanostructured Materials and Characterization Center for Materials and Biology at the University of Texas at Arlington.

References

[1] S. Takei, A. Morisako, M. Matsumoto, J. Magn. Magn. Mater. 272 (2004) 1703–1705.
[2] G.C. Hadjipanayis, W. Tang, Y. Zhang, S.T. Chui, J.F. Liu, C. Chen, H. Kronmuller, IEEE Trans. Magn. 36 (2000) 3382–3387.
[3] H. Zeng, J. Li, Z.L. Wang, J.P. Liu, S. Sun, Nature 420 (2002) 395–398.
[4] G. Sreenivasulu, R. Gopalan, V. Chandrasekaran, G. Markandeyulu, K.G. Suresh, B.S. Murty, Nanotechnology 19 (2008) 335701, 7 pp.
[5] F. Shahzad, S.A. Siddiqi, J. Zhou, Chin. Phys. Lett. 25 (2008) 2642–2644.
[6] G.S. Chaubey, V. Nandwana, N. Poudyal, C.B. Rong, J.P. Liu, Chem. Mater. 20 (2008) 475–478.
[7] Y. Wang, Y. Li, C.B. Rong, J.P. Liu, Nanotechnology 18 (2007) 465701, 4 pp.
[8] K. Gallagher, M. Venkatesan, J.M.D. Coey, IEEE Trans. Magn. 37 (2001) 2528–2530.
[9] V.M. Chakka, B. Altuncevahir, Z.Q. Jin, Y. Li, J.P. Liu, J. Appl. Phys. 99 (2006) 08E912–08E912-3.
[10] Z. Yao, C.B. Jiang, IEEE Trans. Magn. 44 (2008) 4578–4581.
[11] S.K. Chen, M.S. Chu, J.L. Tsai, IEEE Trans. Magn. 32 (1996) 4419–4421.
[12] J. Ding, P.G. McCormick, R. Street, J. Alloys Compd. 228 (1995) 102–104.
[13] L. Li, W.Y. Zhang, Y.Q. Zhou, J.Q. Li, B.G. Shen, J. Zhang, Appl. Phys. Lett. 80 (2002) 2660–2662.
[14] J. Zhang, P. Evans, G. Zangari, J. Magn. Magn. Mater. 283 (2004) 89–91.
[15] J.C. Wei, M. Schwartz, K. Nobe, J. Electrochem. Soc. 55 (2008) D660–D665.
[16] L.J. Pan, D.T. Zhang, M. Yu, Y.C. Li, C. Xu, H.X. Zhang, Rare Met. Mater. Eng. 38 (2009) 161–163.
[17] K. Ono, Y. Kakefuda, Y. Okuda, Y. Ishii, Y. Kamimura, A. Kitamura, M. Oshima, J. Appl. Phys. 91 (2002) 8480–8482.
[18] H.W. Gu, B. Xu, J.C. Rao, R.K. Zheng, X.X. Zhang, K.K. Fung, C.Y.C. Wong, J. Appl. Phys. 93 (2003) 7589–7591.
[19] X. Teng, H. Yang, J. Nanosci. Nanotechnol. 7 (2007) 356–361.
[20] Y. Hou, Z. Xu, S. Peng, C.B. Rong, J.P. Liu, S. Sun, Adv. Mater. 19 (2007) 3349–3352.
[21] Y. Hou, S. Sun, C.B. Rong, J.P. Liu, Appl. Phys. Lett. 91 (2007) 153117–153117-3.
[22] T. Matsushita, T. Iwamoto, M. Inokuchi, N. Toshima, Nanotechnology 21 (2010) 095603, 9 pp.
[23] W.M. Pragnell, H.E. Evans, A.J. Williams, J. Alloys Compd. 473 (2009) 389–393.
[24] W.M. Pragnell, A.J. Williams, H.E. Evans, J. Alloys Compd. 487 (2009) 69–75.
[25] G.T. Landi, A.D. Santos, J. Mater. Sci. 45 (2010) 4906–4911.
[26] Z. Liu, R.J. Chen, Y. Ding, M.Z. Ding, D. Lee, A.R. Yan, J. Appl. Phys. 107 (2010) 09A702–09A702-3;
J.Y. Gu, J. Burgess, C.Y. You, J.Appl. Phys. 107 (2010), 103918–103918-5.
[27] K. Elkins, D. Li, N. Poudyal, V. Nandwana, Z. Jin, K. Chen, J.P. Liu, J. Phys. D: Appl. Phys. 38 (2005) 2306–2309.
[28] C.B. Rong, D. Li, V. Nandwana, N. Poudyal, Y. Ding, Z.L. Wang, H. Zeng, J.P. Liu, Adv. Mater. 18 (2006) 2984–2988.
[29] B.D. Cullity, Introduction to Magnetic Materials, Addison-Wiley, Reading, 1972.
[30] G.S. Chaubey, C. Barcena, N. Poudyal, C.B. Rong, J. Gao, S. Sun, J.P. Liu, J. Am. Chem. Soc. 129 (2007) 7214–7215.
[31] P.E. Kelly, K.O. Grady, P.I. Mayo, R.W. Chantrell, IEEE Trans Magn. 25 (1989) 3881–3886.